

Low- T_c Josephson junctions with tailored barrier

M. Weides, C. Schindler, and H. Kohlstedt

Institute for Solid State Research (IFF) and Center of Nanoelectronic Systems for Information Technology (CNI), Research Centre Juelich, D-52425 Juelich, Germany

(Dated: May 26, 2019)

$Nb=Al_2O_3=N_{0.6}Cu_{0.4}=Nb$ based superconductor-insulator-ferromagnet-superconductor (SIFS) Josephson tunnel junctions with a thickness step in the metallic ferromagnetic $N_{0.6}Cu_{0.4}$ interlayer were fabricated. The step was defined by optical lithography and controlled etching. The step height is on the scale of a few angstroms. Experimentally determined junction parameters by current-voltage characteristics and Fraunhofer pattern indicate an uniform F-layer thickness and the same interface transparencies for etched and non-etched F-layers. This technique could be used to tailor low- T_c Josephson junctions having controlled critical current densities at defined parts of the junction area, as needed for tunable resonators, magnetic-field driven electronics or phase modulated devices.

PACS numbers: 85.25.Cp, 74.50.+r, 74.78.Fk

Keywords: Josephson junctions; superconductor-ferromagnet-superconductor heterostructures, Josephson devices

I. INTRODUCTION

The work horse in superconducting electronics is the Josephson junction. A Josephson junction consists of two weakly coupled superconducting metal bars via a constriction, e.g. made up by a normal (N) metal or a tunnel barrier (I). Various types of Josephson junctions are routinely applied in ultra-high sensitive SQUID (Superconducting Quantum Interference Devices) magnetometers, radio astronomy receivers or the voltage standard [1]. Especially $Nb=Al_2O_3=Nb$ low- T_c tunnel junctions attract considerable interest in many respects. The Al over layer technique [2] allows the fabrication of high density Nb-based Josephson circuits with compromising small parameters spreads. Nonetheless, the Josephson junction itself is a research subject which enriches our understanding of superconductivity, transport phenomena across interfaces and tunnel barriers. Here it is worthwhile to note, that with the advent of high-quality magnetic tunnel junctions approximately 10 years ago, new so far unexplored devices are now under development which make use of both fabrication techniques and which consists of advanced layer sequences compromising superconducting (S) and magnetic materials (F).

At superconductive/magnetic metal (S/F) interfaces the superconducting order parameter ϕ is *spatially decaying and oscillating* inside the magnet (coherence length ξ_F , oscillation length λ_F), whereas for a S/N system ϕ is simply *decaying* inside the metal [3]. By combining the low- T_c Nb=Al technology with magnetic tunnel junctions new functionalities are predicted. In this framework so called 0- Josephson junctions were recent focus of research activities [4, 5, 6].

The supercurrent through an SNS junction is given by $I = I_c \sin(\phi)$, where $\phi = \phi_1 - \phi_2$ is the phase difference of the superconducting electrode wave functions and $I_c > 0$ the maximum supercurrent through the junction [7]. In absence of current ($I = 0$) through the *Josephson junction* (JJ) the

Josephson phase $\phi = 0$ corresponds to the energy minimum. These junctions are so-called 0 JJs. In an SFS stack with ferromagnetic layer thickness $d_F / \xi_F = 2$, the amplitude of order parameter ϕ vanishes at the center of the F-layer and the order parameter has the opposite sign at the adjacent superconducting electrode. This state is described by a phase shift of $\pi/2$ and these junctions are so-called 90° JJs. SFS-type JJs have a negative critical current, hence the Josephson relation can be rewritten: $I = I_c \sin(\phi) = \frac{I_c}{2} \sin(\phi + \pi/2)$ [8, 9]. Recently, these novel types of Josephson junctions have been realized using SFS [10, 11] and SIFS [12, 13] stacks. The kind of coupling can be determined by the $\phi_c(d_F)$ dependence, see Fig. 1.

For a variety of Josephson junctions a non-uniform critical current density ϕ_c is desirable, as for example for tunable superconducting resonators, toy systems for magnetic flux pinning or magnetic-field driven electronic switches similar to SQUIDs. The first considerations [14] of non-uniform ϕ_c 's were caused by technological drawbacks leading to variations of barrier thicknesses by fabrication [15] or of illumination in case of light-sensitive junctions [16]. Later the properties of JJs with periodic spatially modulations were intensively studied regarding the pinning of fluxons [17, 18, 19], the spectrum of electromagnetic waves [20, 21] or their magnetic field dependences [22]. Experimentally the spatial modulation of ϕ_c was realized lithographically by inserting of artificial defects such as insulation stripes across the barrier (ex-situ layer process, $\phi_c = 0$) [23, 24], microshorts (ϕ_c increased) or microresistors (ϕ_c decreased). The properties of JJs depend on geometrical (width, length, thickness) and the physical (dielectric constant of insulator ϵ , resistance R , magnetic thickness d_F and ϕ_c) parameters. When tailoring ϕ_c all other parameters should be unchanged to facilitate calculations and avoid further inhomogeneities in the system. The conventional methods for changing ϕ_c intrinsically modify either R or d_F , too. Our fabrication technology permits the controlled change of only the interlayer thicknesses d_1 and $d_2 = d_1 + d_F$, i.e. the local ϕ_c .

The case of non-uniform coupling phase within a *single* Josephson junction, i.e. one half is a 0 JJ ($d_F = d_1$) and

the other half is a JJ ($d_F = d_2$) (see dashed lines in Fig. 1) is of particular interest. In such a $0-$ junction a spontaneously formed vortex of supercurrent circulating around the $0-$ phase boundary with flux $j_0 = 2j$ inside the JJs may appear [25]. The sign of flux depends on the direction of the circulation and its amplitude equal to $j_0 = 2j$ i.e. a semi-fluxon, if the junction length L is much larger than the Josephson penetration depth ξ [26, 27]. The ground state depends on the symmetry ratios of critical currents $j_c(d_1) \neq j_c(d_2)$ and the effective junction lengths $\ell_1 = \ell_2$ of 0 and π parts ($\ell = L = \xi$). The $0-$ junctions have been actively studied both in theory and experiment during the past few years [6, 28, 29, 30, 31, 32, 33, and references herein]. For the first time $0-$ junctions were studied at so-called tricrystal grain boundaries in d -wave superconductors [28], later in $\text{YCu}_2\text{Cu}_3\text{O}_7\text{-Nb}$ ramp zigzag junctions [30] and Nb based JJ using current injectors [34]. The advantage of SFS/SIFS technology over these systems is that by a proper chosen F-layer thickness d_F the phase can be set to 0 (d_1) or π (d_2) and the amplitude of the critical current densities $j_c(0)$ and $j_c(\pi)$ can be controlled to some degree. It can be prepared in a multilayer geometry (thus allowing topological freedom of design), can be easily combined with the well-developed $\text{Nb}=\text{Al}_2\text{O}_3=\text{Nb}$ technology and has good scalability. For $0-$ junctions one needs 0 and π coupling in *one* junction, setting high demands on the fabrication process, as the change of coupling demands exact control in F-layer thickness. $0-$ JJs have been realized in SFS-like systems [4, 5]. However, both systems have the disadvantages that the $0-$ phase boundary was prepared in a uncontrolled manner and does *not* give information about j_c in 0 and π coupled parts. Hence, the ratios of $j_c(0)/j_c(\pi)$ and ℓ_1/ℓ_2 cannot be calculated for these samples and their ground state is unknown.

In a recent publication [6] the authors presented the first *controllable* stepped $0-$ JJ of SIFS type that are fabricated using high quality $\text{Nb}=\text{Al}_2\text{O}_3=\text{Nb}$ heterostructures. These stepped junctions came along with reference junctions to calculate the ground state of $0-$ JJs. The requirements for SIFS $0-$ junctions are challenging. Here we present our technology background for stepped junctions with the focus on small parameter spreads. Our approach represents a considerable step forward to fulfil the extreme requirements on the implementation of conventional or quantum computing devices based on Josephson junctions.

The current and/or coupling phase profile can be modified by a tailored *stepped* barrier in SXS/SIXS-type ($X=\text{N}, \text{F}$) Josephson junctions. The patterning concept for stepped JJs presented in this article can be either used for JJ with tailored j_c 's and uniform phase $0-0$ ($-\pi$) JJs (dots in Fig. 1) or with symmetric j_c 's and non-uniform phase, i.e. $0-$ JJs (dashes in Fig. 1).

II. EXPERIMENT

A Leybold Univex 450b magnetron sputter system with 8 targets in the main chamber, a load-lock including an etching stage, as well as a separate oxidation chamber was used for

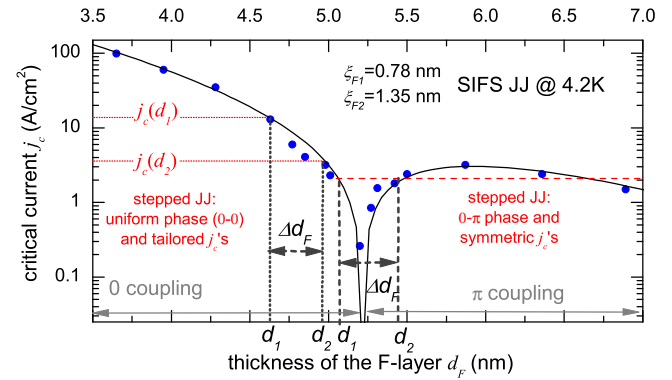


FIG. 1: (color online) $j_c(d_F)$ dependences and fitting curve for SIFS-JJs. F-layer thicknesses chosen as d_1 and d_2 in stepped JJs yields $0-0$ coupled junction with asymmetry in j_c (dotted lines) or symmetric $0-$ junction (dashed lines). Data from Ref. [13].

TABLE I: Deposition (DC-sputtering) and etching parameters for SIFS stacks. The rates were determined by profiler measurements.

metal	Ar pressure [10^{-3} m bar]	power density [W = cm ⁻²]	rate [nm = s]	parameters
Nb	7.0	5	2.0	static
Al	7.0	1.9	0.05	rotation
NiCu	4.2	0.6	0.34	target shifted
Cu	4.2	1.9	0.1	rotation
SF ₆ on Nb	15	0.6	1	RF-source
SF ₆ on NiCu	15	0.6	< 0.001	RF-source
Ar on NiCu	5	0.6	0.01	RF-source

the junction preparation. Together with a transfer chamber, a robot handler and a Siemens Simatic control unit, the cluster tool is able to deposit automatically (pre-programmed) tunnel junction layer sequences for superconducting and spintronics applications.

The deposition and patterning of the stepped SIFS junctions was performed by a four level photolithographic mask procedure. Here we present an improved version of an earlier fabrication sequence for planar SIS junctions [2]. A magnetron sputtering system capable of handling 4-inch wafers and a background pressure of 5×10^{-7} m bar was used. Nb and NiCu were statically deposited, while Al and Cu were deposited during sample rotation and at much lower deposition rates to obtain very homogeneous and uniform films, see table I. Although the actual stack sequence for the junctions is SINFS, the N-layer (Cu) was introduced to provide the growth of an uniform and homogenous F-layer thickness [35]. It is not relevant for the electric and magnetic properties discussed here and will be neglected.

The F-layer was deposited with a gradient of thickness along y-axis on the S/I stack [35]. The increase of thickness over the junctions width (~ 100 nm) is estimated as less than

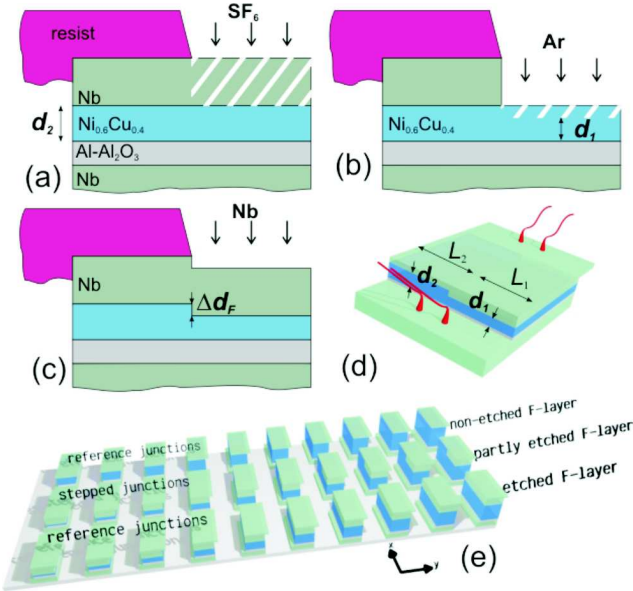


FIG. 2: (color online) The complete SIFS stack was protected in part by photoresist. The Cu-layer was necessary for uniform current transport: (a) reactive etching of Nb with SF_6 down to NiCu layer, (b) ion-etching of NiCu to set I_c coupling, (c) in situ deposition of cap Nb layer. Schematic layouts of stepped JJ based on SFS/SIFS technology (d) and of stepped JJ along with planar reference junctions (e). The F-layer (blue) thickness increases from left to right.

0.02 nm, i.e. the F-layer can be treated as planar for an individual junction. After the deposition of 40 nm Nb as cap layer and subsequent lift-off the complete SIFS stack with wedge-shaped F-layer thickness, but without steps in F-layer, was obtained.

The patterning of the desired step-like variation in d_F was done after the complete deposition of the SIFS stack. The parts of the JJ that were supposed to have a larger thickness d_2 were protected by photoresist, see Fig. 2. Ion-etching alone of both Nb and NiCu to define the step in F-layer did not provide a good control over the final F-layer thickness, as this unselective and long-timed etching has the disadvantages of non-stable etching rates and an non-uniform etching front. Therefore it was not possible to achieve in such way a defined step.

The use of selective etching in $\text{Nb}=\text{Al}_2\text{O}_3=\text{Nb}$ stack fabrication processes, such as CF_4 and SF_6 reactive ion etching (RIE) or other techniques are reported in Ref. [36]. In particular, it was shown that SF_6 provides an excellent RIE chemistry for low-voltage anisotropic etching of Nb with high selectivity towards other materials. The inert SF_6 dissociated in a RF-plasma and the fluor diffused to the surface of the substrate, where it reacted with niobium $5\text{F} + \text{Nb} \rightarrow \text{NbF}_5$. The volatile NbF_5 was pumped out of the etching-chamber. When SF_6 was used as process gas all non-metallic etching products such as fluorides and sulfides from the top-layer of the NiCu-layer had to be removed by subsequent argon etching.

The patterning process of the step is depicted in Fig. 2 (a)-

(c). The key points were i) *selective reactive etching* of Nb, ii) *argon etching* of NiCu to define $d_1 = d_2 - d_F$ and iii) subsequent *in situ* deposition of Nb.

The Nb cap layer was removed by reactive dry etching using SF_6 with a high selectivity to the photoresist (AZ5214E). A few tenth of nanometer NiCu were Ar ion etched at a very low power and rate to avoid any damaging of the NiCu film under the surface and to keep a good control over the step height. When the F-layer thickness was reduced down to the thickness d_1 the etching was stopped and 40 nm of Nb were deposited. The complete etching and subsequent Nb deposition was done *in situ* at a background pressure below 2×10^{-6} mbar. The chip contained stacks with the new F-layer thicknesses d_1 (uniformly etched), d_2 (non-etched) and with step in the F-layer thickness from d_1 to d_2 .

After the preparation of steps in F-layer the actual junction areas were defined by aligning the photo mask on the visible step-terraces (ramp of 20 nm height and 1 m width), followed by Ar ion-beam etching of the upper Nb, NiCu and Al layers. The length L_1 and L_2 of a stepped junction are within lithographic alignment accuracy of 1 m. The etching was controlled by a secondary ion mass spectrometry (SIMS) and stopped after the complete etching of the Al_2O_3 tunnel barrier. Afterwards the mesas were insulated by SNEAP (Selective Niobium Etching and Anodization Process) [2]. In the last photolithographic step the wiring layer was defined. After a short argon etching to reduce the contact resistance a 300 nm thick Nb wiring was deposited. Fig. 2 (d) sketches a stepped SIFS junction and (e) the completely structured chip with sets of stepped and planar reference junctions and wedge shaped F-layer along y-axis. Fig. 1 depicts the I_c (d_F) dependence of planar SIFS JJs with NiCu as ferromagnetic interlayer. Note that a simple decay of I_c can generally be achieved by increasing the interlayer thickness, independent of its magnetic properties, i.e. in SNS or SINS junctions. The wedge shaped interlayer (Fig. 2 (e)) facilitates the quick fabrication of samples with various F-layer thickness and, at the same time, a low junction to junction deviation.

III. RESULTS AND DISCUSSION

On test samples multiple steps with 2 m gaps were structured for analysis with scanning electron (SEM) and atomic force (AFM) microscopy after etching and Nb deposition, see Fig. 3. For SEM the photoresist was left on the sample and for AFM it was removed. While etching with SF_6 the NiCu-layer served as an etching barrier. Thus, it facilitated the over-etching of the Nb to ensure its complete removal despite the shadow effects from resist walls (1 m height). The short-timed argon etched NiCu-layer was slightly non-uniform near the resist walls due to the anisotropic etching front. Since in real stepped JJs the half with $d_F = d_1$ has dimensions about 10 m or larger, the non-uniformity of the NiCu layer near the step, created by shadow-effects of the resist, was averaged out in transport measurements. The presence of resist caused a decrease of the Nb deposition rates by 10%, espe-

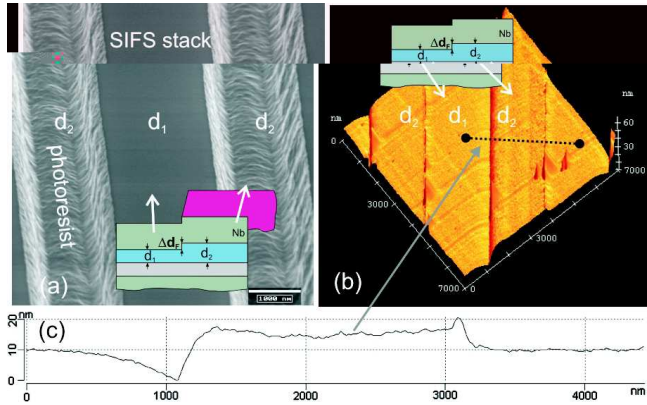


FIG. 3: (color online) Topography of test sample with multiple steps and 2 m wide gaps after etching and Nb deposition. (a) SEM image before removal of photoresist (protecting coupled parts); (b) AFM image (7 m^2) after removal of photoresist; (c) Profile measured by AFM (dotted line).

cially near the asymmetric resist walls (seen in SEM). Thus, the non-uniform deposition of Nb after the reactive and argon etching led to a non-uniform cap layer, seen in the difference of stack heights (much larger than d_F) in the AFM image of the SIFS stack, Fig. 3(b).

On planar SIFS-JJs (reference junctions) the actual step height d_F and the coupling is estimated by comparing $j_c(d_1)$ with the known $j_c(d_F)$ dependence, see Fig. 1. d_2 is determined from a reference sample with wedge-shaped F-layer. Our experimental results suggested that a continuously variable-thickness model was more suitable for the junctions than a monolayers-thickness model (radius of neutral NiCu is 0.15 nm) [37].

By the IVC and $I_c(H)$ of the reference JJs one can estimate parameters for the stepped junction, such as the ratio of asymmetry $j_c(d_1)/j_c(d_2)$ and the quality of the etched and non-etched parts. The uniformity of the supercurrent transport in a Josephson junction can be judged qualitatively from the magnetic field dependence of the critical current $I_c(H)$. The magnetic field H was applied in-plane and along one junction axis. The magnetic diffraction pattern depends in a complex way on the effective junction length and on the current distribution over the junction area [38]. The ideal pattern of a short (< 1) JJ is symmetric with respect to both polarities of the critical current and the magnetic field with completely vanishing I_c at the minima. If the pattern is not symmetric, irregular or has a current offset, the current transport over the non-superconducting interlayers is non-uniform. If the trapping of magnetic flux can be excluded this effect is attributed to non-uniformity of the tunnel barrier, the ferromagnetic layer or the interface transparencies over the junction area.

A. Reference junctions

Fig. 4 shows IVC and $I_c(H)$ dependences for a non-etched junction (dot) with the F-layer thickness $d_2 = 5.05\text{ nm}$

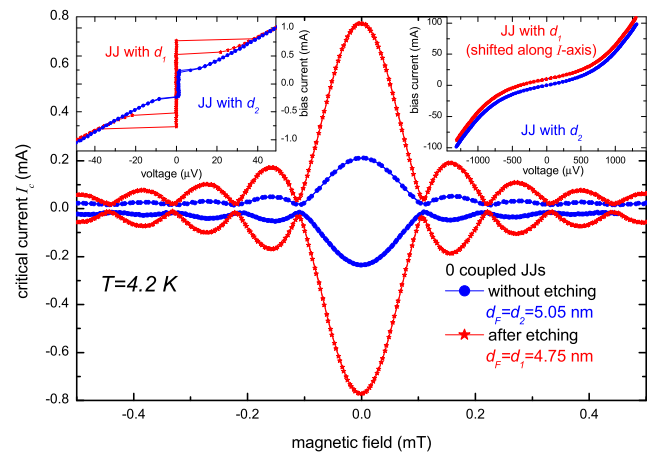


FIG. 4: (color online) $I_c(H)$ of etched (star) and non-etched (dots) JJs. The insets show IVCs for small and large bias current ranges in zero magnetic field. Both JJs are in the short JJ limit. Measurements were done at 4.2 K .

and a uniformly etched junction (star) with thickness $d_1 = d_2 = d_F = 4.75\text{ nm}$. Both junctions were 0 coupled. The step height $d_F = 0.3\text{ nm}$ is calculated by comparing $I_c(d_1)$ with $j_c(d_F)$ from Fig. 1. The polycrystalline structure of the room-temperature sputtered layers and the very low etching rate of NiCu led to a good control over d_F : However, one has to keep in mind that the local variation of F-layer thickness might exceed this value, and the values for d_1 , d_2 and d_F are just the mean thicknesses seen by the transport current. The insets of Fig. 4 show the IVCs for small and large ranges of bias current. Besides the difference in I_c , the $I_c(H)$ dependence and the IVCs (right inset) showed no evidence for an inhomogeneous current transport for both samples. The larger I_c , but same resistance R and capacitance C led to a slightly hysteretic IVC of the etched sample, as the width of hysteresis is determined by McCumber parameter $c = I_c^2 R C$. The resistance R is nearly independent from d_F as the voltage drop over the tunnel barrier is much larger than the serial resistance of a few nanometer thick metal [13]. However, an etching-induced change of transparency at the F/S interface might modify R . No change of R is visible in the IVCs of both JJs in Fig. 4, apart from the change in I_c . A change of capacitance C would require a change of R , as both are determined by the dielectric tunnel barrier.

The scattering of the critical current I_c and resistance R on the etched junctions was, just like for the non etched SIFS junctions, of the order of 2%. The trapping of magnetic flux might cause a larger variation in critical current density than the interface asymmetry stemming from the etching process. For all thicknesses of ferromagnetic layer the same homogeneity of the etched junctions were observed.

A set of junctions denoted by the dashes in Fig. 1 was measured by the authors, too. The $I_c(H)$ dependences of this 0, and 0– JJs are depicted in Fig. 3 of Ref. [6]. These junctions show the same quality of parameters for the etched and non-etched samples as the samples depicted in Fig. 4.

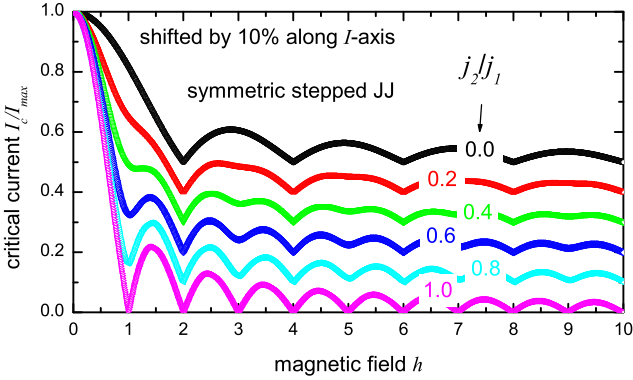


FIG. 5: (color online) Calculated $I_c(h)$ dependence for various ratios of $j_2=j_1$ and centered step in j_c profile.

B. Stepped junctions

1. Calculated $I_c(h)$ of stepped JJ

The magnetic diffraction pattern $I_c(H)$ of a JJ depends on its j_c profile, see Ref. [38]. The analytic solution for a short ($\lambda < 1$) stepped junction with different critical current density j_1 and j_2 in both halves is given by

$$I_c(h) = \frac{j_1 \cos(\phi_0 - h) - j_2 \cos(\phi_0 + h) + (j_2 - j_1) \cos 2h}{2h},$$

where ϕ_0 is an arbitrary initial phase, $h = 2\pi \phi_0 L H = \phi_0$ the normalized magnetic flux through the junction cross section, L the magnetic thickness of junction and A the junction area. The phase-field relation for maximum I_c is reached for

$$\phi_0 = \arctan \left[\frac{j_2 h \sin h - j_1 h \sin h}{2h j_2 \sin^2 \frac{h}{2} + 2h j_1 \sin^2 \frac{h}{2}} \right];$$

The calculated $I_c(h)$ for various ratios of $j_2=j_1$ is depicted in Fig. 5. Characteristic features are the centered maximum peak and the appearance of periodic minima of the supercurrent for $h = n$ for integer n . The height of the odd-order minima ($n = 1, 3, 5, \dots$) depends on the asymmetry ratio $j_c(d_2) = j_c(d_1)$ and increases for decreasing $j_c(d_2)$. $I_c(h)$ is completely vanishing for magnetic flux equal to multiples of $2\pi\phi_0$. The maximum critical current at $I_c(0)$ decreases linearly down to $I_c = I_{c, \text{max}} = 0.5$ for $j_c(d_2) = 0$. The corresponding $I_c(h)$ pattern becomes that of a junction with half the width and uniform j_c .

2. Measured $I_c(H)$ of stepped JJ

In Fig. 6 the measured magnetic diffraction pattern $I_c(H)$ of a stepped JJ along with calculated $I_c(h)$ curves are depicted. Both junction halves are 0 coupled. The magnetic field axis h was scaled to fit the first measured minima of $I_c(H)$. d_F is determined by comparing j_c of reference junction with the known $j_c(d_F)$ dependence in Fig. 1, yielding

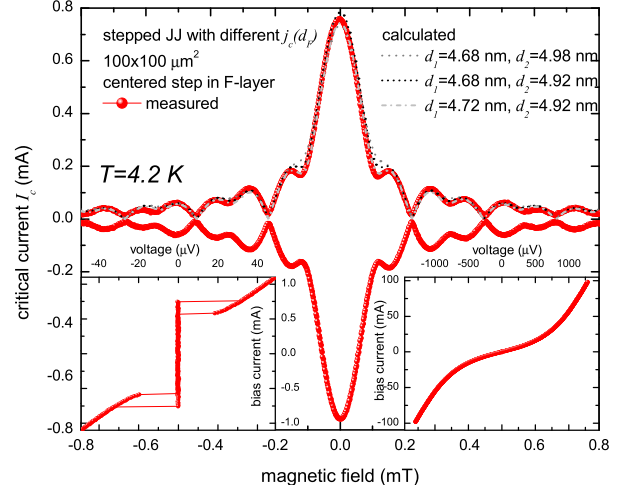


FIG. 6: (color online) $I_c(H)$ of a stepped 0-0 JJs (square shaped with $100\text{ }\mu\text{m}$ junction length) with $d_1 = 4.68\text{ nm}$ and $d_2 = 4.98\text{ nm}$ (determined from reference JJs) plus calculated $I_c(h)$. The junction is in short JJ limit.

$d_1 = 4.68\text{ nm}$ and $d_2 = 4.98\text{ nm}$. Due to the rather steep slope of the $j_c(d_F)$ curve near the 0 to crossover at $d_F = 5.21\text{ nm}$, j_c is very sensitive to d_1 and d_2 . A variation of d_1 and d_2 by 0.05 nm changes j_c up to 30%. The sputter rate may vary slightly over the $500\text{ }\mu\text{m}$ distance to the reference junctions, preventing the exact estimation of d_1 and d_2 . We calculated $I_c(h)$ (dashes) using $d_1 = d_2 = d_F = 4.68\text{ nm}$ and $d_2 = 4.98\text{ nm}$ determined from reference junctions. Then d_2 was decreased by 0.04 nm (dots) and finally d_F increased by the same thickness, too (dash-dots). The final calculation has the best agreement with data, although the total interface roughness (rms) of the multilayers should exceed 0.04 nm by far. The measurement and simulation in Fig. 6 show the good estimation and control of F-layer thicknesses.

IV. CONCLUSIONS

Josephson junctions with a step in the ferromagnetic layer were fabricated. Using a wedge-shaped F-layer in a SIFS stack on a 4-inch wafer along with stepped and reference junctions it was possible to trace out regimes of different couplings ($0, \pm 1, \dots$), depending on the initial F-layer thickness d_F and step d_F . The etched and non etched SIFS junctions differ only by F-layer thickness. No inhomogeneities can be seen in the current transport characteristics of the etched junctions.

The patterning of stepped Josephson junctions allows free lateral placement of well-defined j_c 's and/or local coupling regimes within a single junction. If decreasing temperature the slope $\partial j_c / \partial T$ depends on the interlayer thickness (observed in SIFS JJs [13]), and the ratio $j_1 = j_2$ could be varied

thermally. Stepped junctions can be realized in Nb based JJs with any interlayer material (N,F,I) which is chemically stable towards the reactive etching gas. The patterning process could be adjusted to all thin film multilayer structure providing that the reactive etching rates of the layer materials differ. Replacing the optical lithography with electron beam lithography may enhance the lateral accuracy of the step down to the dimension of e-beam and decrease the non-uniformity near the resist wall due to the thinner resist height.

JJs with varying β_c and planar phase could be used for devices with special shaped $T_c(H)$ pattern [38], toy systems for flux pinning or tunable superconducting resonators. $0-$ JJs based on low- T_c superconductors with stepped F-layer offer a great flexibility for the integration of this devices, as it offers advantages over the existing $0-$ junctions based on d-wave superconductors [30, 39] or current injectors [34] such as the low dissipation of plasma oscillations, no restrictions in topology, no additional bias electrodes and easy integration into the mature Nb-Al₂O₃-Nb technology.

The $0-$ SIFS JJs with stepped F-layer allow to study the physics of fractional vortices with a good control of the ratio of symmetry between 0 and π parts. The change in magnetic diffraction pattern between short to the long $0-$ JJ limit [29] or the formation of spontaneous flux in the ground state of multiple $0-$ phase boundaries in a long JJ could be studied [32]. $0-$ JJs may be used as the active part in the qubit, as was recently proposed [33].

Acknowledgement

The authors thank B. Hermanns for help with fabrication and E. Goldobin, R. Kleiner, D. Koelle and A. Ustinov for fruitful discussions. This work was supported by ESF program PiShift and Heraeus Foundation.

[1] W. Buckel and R. Kleiner, *Superconductivity. Fundamentals and Applications.*, Wiley-VCH (2004).

[2] M. Gurvitch, M. A. Washington, H. A. Huggins and J. M. Rowell, *IEEE Trans. Magn.* **19**, 791 (1983).

[3] A. I. Buzdin, *Rev. Mod. Phys.* **77**, 935 (2005).

[4] M. L. Della Rocca, M. Aprili, T. Kontos, A. Gomez and P. Spatschek, *Phys. Rev. Lett.* **94**, 197003 (2005).

[5] S. M. Frolov, D. J. Van Harlingen, V. V. Bolginov, V. A. Oboznov and V. V. Ryazanov, *Phys. Rev. B* **74**, 020503 (2006).

[6] M. Weides, M. Kemmler, E. Goldobin, H. Kohlstedt, R. Waser, D. Koelle and R. Kleiner, *Phys. Rev. Lett.* **12**/2006, cond-mat/0605656

[7] B. D. Josephson, *Phys. Lett.* **1**, 251 (1962).

[8] L. Bulaevskii, V. Kuzii and A. Sobyanin, *JETP Lett.* **25**, 7 (1977).

[9] A. I. Buzdin and M. Yu. Kupriyanov, *JETP Lett.* **53**, 321 (1991).

[10] A. V. Veretennikov, V. V. Ryazanov, V. A. Oboznov, A. Yu. Rusanov, V. A. Larkin and J. Aarts, *Physica B* **284**, 495 (2000).

[11] Y. Blum, A. Tsukernik, M. Karpovski and A. Palevski, *Phys. Rev. Lett.* **89**, 187004 (2002).

[12] T. Kontos, M. Aprili, J. Lesueur and X. Grison, *Phys. Rev. Lett.* **89**, 137007 (2002).

[13] M. Weides, M. Kemmler, E. Goldobin, D. Koelle, R. Kleiner, H. Kohlstedt and A. Buzdin, *Appl. Phys. Lett.* **89**, 122511 (2006).

[14] M. Russo and R. Vaglio, *Phys. Rev. B* **17**, 2171 (1978).

[15] K. Schwidal and R. D. Finnegan, *J. Appl. Phys.* **40**, 213 (1969).

[16] A. Barone, G. Paternò, M. Russo, and R. Vaglio, *Phys. Stat. Solidi (a)* **41**, 393 (1977).

[17] D. W. McLaughlin and A. C. Scott, *Phys. Rev. B* **18**, 1652 (1978).

[18] A. N. Vystavkin, Yu. F. Drachevskii, V. P. Koshelets and I. L. Serpuchenko, *Sov. J. Low Temp. Phys.* **14**, 357 (1988).

[19] B. A. Malomed and A. V. Ustinov, *J. Appl. Phys.* **67**, 3791 (1990).

[20] M. V. Fistul, P. Caputo and A. V. Ustinov, *Phys. Rev. B* **60**, 13152 (1999).

[21] N. Lazarides, *Supercond. Sci. Technol.* **18**, 73 (2005).

[22] N. Lazarides, *Phys. Rev. B* **68**, 92506 (2003).

[23] A. Golubov, A. Ustinov and I. L. Serpuchenko, *Phys. Lett. A* **130**, 107 (1988).

[24] M. A. Itzler and M. Tinkham, *Phys. Rev. B* **51**, 435 (1995).

[25] L. N. Bulaevskii, V. V. Kuzii and A. A. Sobyanin, *Solid State Commun.* **25**, 1053 (1978).

[26] J. H. Xu, J. H. Miller and C. S. Ting, *Phys. Rev. B* **51**, 11958 (1995).

[27] E. Goldobin, D. Koelle and R. Kleiner, *Phys. Rev. B* **66**, 100508 (2002).

[28] C. C. Tsuei and J. R. Kirtley, *Rev. Mod. Phys.* **72**, 969 (2000).

[29] J. R. Kirtley, K. A. Moler and D. J. Scalapino, *Phys. Rev. B* **56**, 886 (1997).

[30] H. Hilgenkamp, Ariando, H. J. H. Smilde, D. H. A. Blank, G. Rijnders, H. Rogalla, J. R. Kirtley and C. C. Tsuei, *Nature (London)* **422**, 50 (2003).

[31] E. Goldobin, D. Koelle and R. Kleiner, *Phys. Rev. B* **67**, 224515 (2003).

[32] A. Zenchuk and E. Goldobin, *Phys. Rev. B* **69**, 024515 (2004).

[33] E. Goldobin, K. Vogel, O. Crasser, R. Walser, W. P. Schleich, D. Koelle and R. Kleiner, *Phys. Rev. B* **72**, 054527 (2005).

[34] E. Goldobin, A. Sterck, T. Gaber, D. Koelle and R. Kleiner, *Phys. Rev. Lett.* **92**, 057005 (2004).

[35] M. Weides, K. Tillmann and H. Kohlstedt, *Physica C* **437-438**, 349 (2006).

[36] A. W. Lichtenberger, D. M. Lea and F. L. Lloyd, *IEEE Trans. Appl. Supercond.* **3**, 2191 (1993).

[37] M. Weides, Ph. D. thesis, Universität zu Köln, Germany (2006).

[38] A. Barone and G. Paterno, *Physics and Applications of the Josephson Effect*, John Wiley & Sons (1982).

[39] J. R. Kirtley, C. C. Tsuei, M. Rupp, J. Z. Sun, L. S. Yu-Jahnes, A. Gupta, M. B. Ketchen, K. A. Moler and M. Bhushan, *Phys. Rev. Lett.* **76**, 1336 (1996).